

ROME1-1178/97
July 1997

Measuring $Z\gamma H$ vertex effects at $e\gamma$ linear colliders.

E. Gabrielli ^a, V.A. Ilyin ^b and B. Mele ^c.

^a University of Notre Dame, IN, USA

^b Institute of Nuclear Physics, Moscow State University, Russia

^c INFN, Sezione di Roma 1 and Rome University “La Sapienza”, Italy

Abstract

The one-loop process $e\gamma \rightarrow eH$, for intermediate Higgs masses is considered. Exact cross sections for unpolarized and longitudinally polarized beams are computed and found to be more than two orders of magnitude larger than the rates for the crossed process $e^+e^- \rightarrow H\gamma$, in the energy range $\sqrt{s} = (0.5 \div 2)$ TeV. We show that, apart from being competitive with the $\gamma\gamma \rightarrow H$ process for testing the one-loop $\gamma\gamma H$ vertex, by requiring a final electron tagged at large angle the channel $e\gamma \rightarrow eH$ provides an excellent way of testing the $Z\gamma H$ vertex.

e-mail:

egabriel@wave.phys.nd.edu, ilyin@theory.npi.msu.su, mele@roma1.infn.it

To appear in the Report DESY 97-123E

Possible ways to test the one-loop couplings ggH , $\gamma\gamma H$ and $Z\gamma H$ have been extensively studied in the literature. Because of the nondecoupling properties of the Higgs boson, these vertices are sensitive to the contribution of new particles circulating in the loops, even in the limit $M_{new} \gg m_H$ [1]. A measurement of the $\gamma\gamma H$ and $Z\gamma H$ couplings should be possible by the determination of the BR's for the decays $H \rightarrow \gamma\gamma$ [2, 3] and $H \rightarrow \gamma Z$ [4, 3], respectively. This is true only for an intermediate-mass Higgs boson (i.e., for $90\text{GeV} \lesssim m_H \lesssim 140\text{ GeV}$), where both $\text{BR}(H \rightarrow \gamma\gamma)$ and $\text{BR}(H \rightarrow \gamma Z)$ reach their maximum values, which is $\mathcal{O}(10^{-3})$.

Another promising way of measuring the $\gamma\gamma H$ coupling for an intermediate-mass Higgs boson will be realized through the Higgs production in $\gamma\gamma$ collisions [5, 6]. To this end, the capability of tuning the $\gamma\gamma$ c.m. energy on the Higgs mass, through a good degree of the photons monochromaticity, will be crucial for not diluting too much the $\gamma\gamma \rightarrow H$ resonant cross section over the c.m. energy spectrum.

In this short note, we sum up the main results recently obtained on the Higgs production in $e\gamma$ collisions through the one-loop process $e\gamma \rightarrow eH$ [7]. This channel turns out to be an excellent means to test both the $\gamma\gamma H$ and $Z\gamma H$ one-loop couplings with relatively high statistics, without requiring a fine tuning of the c.m. energy. While the γ -exchange $\gamma\gamma H$ contribution is dominant in the total cross section, by requiring a large transverse momentum of the final electron (or Higgs boson), one enhances the Z -exchange $Z\gamma H$ contribution, while keeping the corresponding rate still to an observable level. The further contribution given by the box diagrams with W and Z exchange survives at large angles too, but is relatively less important. Furthermore, while the $\gamma\gamma H$ and $Z\gamma H$ channels increase logarithmically with the c.m. collision energy, the contribution from boxes starts decreasing at $\sqrt{s} \gtrsim 400\text{ GeV}$.

In our study we assumed that the initial photon beam is to a good degree monochromatic, and has an integrated luminosity of $\mathcal{O}(100)\text{ fb}^{-1}$.

The cross section for the process $e\gamma \rightarrow eH$ has previously been studied in the Weizsäcker-Williams (WW) approximation [8], where the only channel contributing is the (almost real) γ -exchange in the t -channel, induced by the $\gamma\gamma H$ vertex [9]. This method provides a rather good estimate of the $e\gamma \rightarrow eH$ total cross sections, but it is unable to assess the importance of the $Z\gamma H$ (and box) effects. This we will address particularly in our exact treatment of $e\gamma \rightarrow eH$.

Although, the cross sections for the process $e\gamma \rightarrow eH$ are quite large also for heavy Higgs masses, we will concentrate on the intermediate Higgs mass case (hence, assuming that the decay $H \rightarrow b\bar{b}$ is dominant).

The crossed process, $e^+e^- \rightarrow H\gamma$, has been studied in different papers [10, 11, 12]. However, the $e^+e^- \rightarrow H\gamma$ channel suffers from small rates, which are further depleted at large energies by the $1/s$ behavior of the dominant s-channel diagrams. As a consequence, if a $e\gamma$ option of the linear collider will be realized with similar luminosity of the e^+e^- option, the $e\gamma \rightarrow eH$ channel will turn out to be much more interesting than the process $e^+e^- \rightarrow H\gamma$ for finding possible deviations from the standard-model one-loop Higgs vertices.

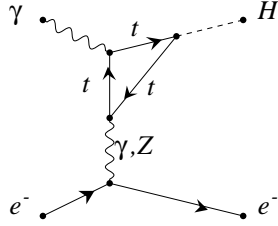


Figure 1: Feynman diagram with fermion triangle loop.

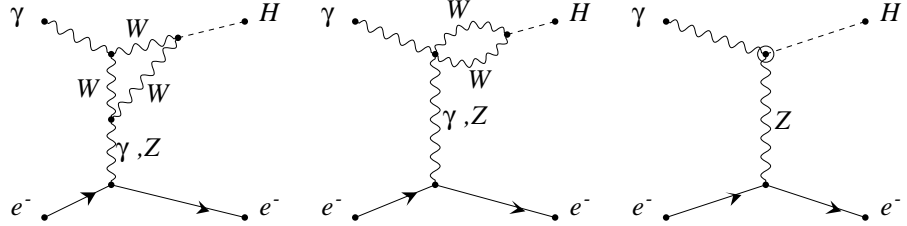


Figure 2: Feynman diagrams with W -triangle loop.

In [7], we present the complete analytical results for the helicity amplitudes of the $e\gamma \rightarrow eH$ process (see also [13]). Although, we have calculated the relevant amplitudes for the process $e\gamma \rightarrow eH$ in the 't-Hooft-Feynman gauge, for brevity we show the corresponding Feynman diagrams in the unitary gauge (figures 1–4).

In figure 6, the total (unpolarized) cross sections for the one-loop process $e\gamma \rightarrow eH$ and the tree-level Higgs production $e\gamma \rightarrow H\nu_e W$ (computed by CompHEP [14]) are plotted versus m_H , for $\sqrt{s} = 500$ and 800 GeV. One can see that the process $e\gamma \rightarrow eH$ is characterized by relatively large rates. For instance, for m_H up to about 400 GeV, one finds $\sigma(He) > 1$ fb, which, for an integrated luminosity of about 100 fb^{-1} , corresponds to more than 100 events.

A possible strategy to enhance the $Z\gamma H$ vertex effects (depleted by the Z propagator) with

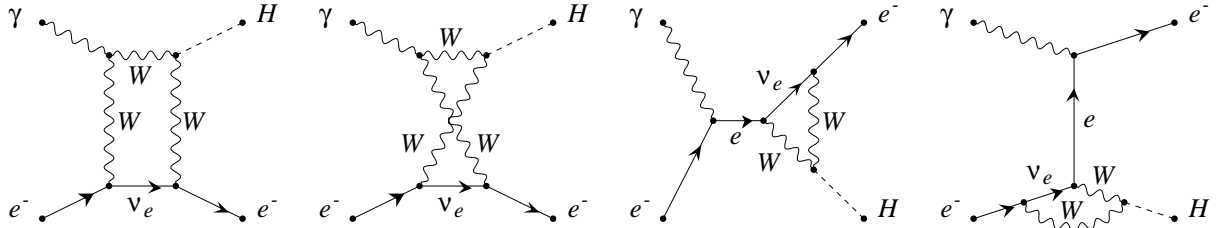


Figure 3: Subset of Feynman diagrams with W -box loop and related eeH vertex.

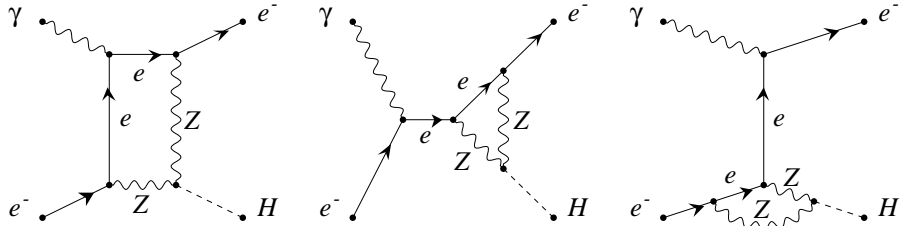


Figure 4: Subset of diagrams with Z -box loop and related eeH vertex.

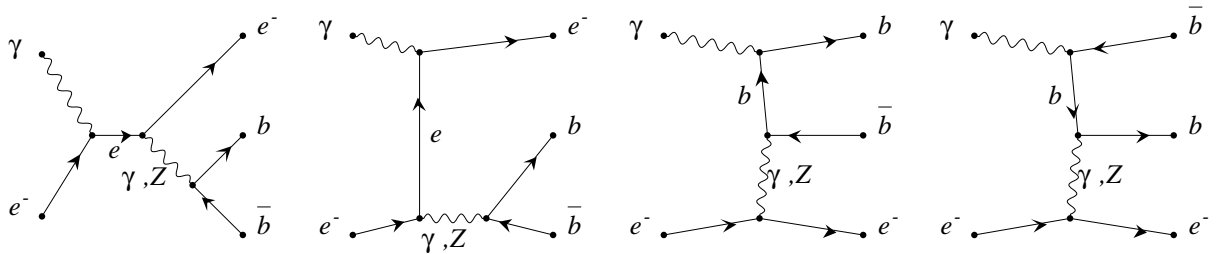


Figure 5: Diagrams for the $e\gamma \rightarrow ebb\bar{b}$ background.

respect to the dominant $\gamma\gamma H$ contribution in the He production rate consists in requiring a final electron tagged at large angle. The corresponding cut on the transferred squared momentum t depletes mainly the amplitudes involving a photon propagator in the t channel. This can be easily seen from the two plots in figure 7, where the cross sections dependence on \sqrt{s} , for $m_H = 120\text{GeV}$, is shown for no cut on the electron transverse momentum p_T^e (a), and a cut $p_T^e > 100\text{GeV}$ (b). We show separately the contributions to the cross section given by the squared amplitudes corresponding to the subsets of Feynman diagrams “ $\gamma\gamma H$ ”, “ $Z\gamma H$ ” and “BOX” (as defined in [7]). Even if this separation is by no means formally rigorous (and neglects the relative interference effects), it can help in getting a feeling of the relative importance of the triangular vertices and box contributions to the total cross section. One can see that the relative weight of the $Z\gamma H$ and BOX contributions with respect to the total cross section is considerably enhanced by a cut on the minimum allowed p_T^e . For $p_T^e > 100\text{GeV}$, $Z\gamma H$ is about 60% of $\gamma\gamma H$, and $Z\gamma H$ gives a considerable fraction of the total production rate, which still is sufficient to guarantee investigation (about 0.7 fb). One can also notice that the BOX contribution is of some relevance only in the lower \sqrt{s} range.

Note that in the inclusive He production, the bulk of the events are characterized by a forward final electron escaping detection. On the other hand, requiring a large p_T^e corresponds, from an experimental point of view, to selecting a different final-state configuration, where the Higgs decay products have a large total transverse momentum, balanced by a high-energy electron detected at large angle.

In principle, the $e\gamma \rightarrow eH$ total cross section (and its main contribution from $\gamma\gamma H$) is of the same order of magnitude of the total rates for Higgs production in $\gamma\gamma$ collisions [6]. Indeed, the

expected resolution on the beam energy smears the higher peak cross section over a width much larger than the Higgs resonance. As a result, the channel $e\gamma \rightarrow eH$ has a comparable potential with respect to the process $\gamma\gamma \rightarrow H$ in testing the $\gamma\gamma H$ vertex, as far as the production rates are concerned. In our work, on the other hand, we concentrated on the problem of disentangling the $Z\gamma H$ vertex effects, which are out of the $\gamma\gamma$ -collision domain.

The main irreducible background to the process $e\gamma \rightarrow eH \rightarrow e(b\bar{b})$ comes from the channel $e\gamma \rightarrow e b\bar{b}$. The corresponding set of Feynman diagrams is given by 8 graphs and is shown in figure 5. A crucial parameter to set the importance of the $e\gamma \rightarrow e b\bar{b}$ background is the experimental resolution on the $b\bar{b}$ invariant mass $\Delta m_{b\bar{b}}$. The background rates we present here are obtained by integrating the $m_{b\bar{b}}$ distribution over the range $m_H - \Delta m_{b\bar{b}} < m_{b\bar{b}} < m_H + \Delta m_{b\bar{b}}$, assuming $\Delta m_{b\bar{b}} = 3\text{GeV}$. We used CompHEP to generate the $e\gamma \rightarrow e b\bar{b}$ kinematical distributions and cross sections. The background rates turn out to be considerably larger than the signal, especially at moderate values of p_T^e . The situation can be improved by putting a cut on the angles between each b and the initial beams. In fact, the vector couplings that characterize the b 's in the channel $e\gamma \rightarrow e b\bar{b}$ give rise to a b angular distribution considerably more forward-backward peaked than in the case of the scalar $Hb\bar{b}$ coupling relevant for the signal.

In table 1, the signal and background rates are reported, when an angular cut $\theta_{b-beam} > 18^\circ$ is applied between each b quark and both the beams for two different sets of p_T^e cuts, that enhance the $Z\gamma H$ contribution, and $m_H = 120\text{ GeV}$, at $\sqrt{s} = 500\text{ GeV}$. The assumed θ_{b-beam} cut reduces the signal and background distributions at a comparable level, without penalizing appreciably the signal rate at large p_T^e . Note that the cut $\theta_{b-beam} > 18^\circ$ has been optimized at $\sqrt{s} = 500\text{GeV}$. Lower angular cuts will be more convenient at larger \sqrt{s} . Different initial polarizations for the e beam are also considered (see below).

A further source of background for the process $e\gamma \rightarrow eH \rightarrow e(b\bar{b})$ is the charm production through $e\gamma \rightarrow ec\bar{c}$, when the c quarks are misidentified into b 's. This reducible background can be cured by a good b -tagging efficiency, that should control a charm production rate that can be even more than a factor 10 larger than the corresponding $e\gamma \rightarrow e b\bar{b}$ cross section, depending on the particular kinematical configuration [9]. We computed the rate for $e\gamma \rightarrow ec\bar{c}$. By assuming a 10% probability of misidentifying a c quark into a b (hence, considering only a fraction 1/10 of the computed $e\gamma \rightarrow ec\bar{c}$ rate), we find that this reducible background has lower rates than the irreducible one. This can be also seen in table 1. Note that the $e\gamma \rightarrow ec\bar{c}$ channel is kinematically similar to $e\gamma \rightarrow e b\bar{b}$. Hence, the particular strategies analyzed here to reduce the latter automatically depletes also the former. For unpolarized beams and $p_T^e > 100\text{GeV}$, the $e\gamma \rightarrow ec\bar{c}$ “effective rate” is less than 1/3 of the $e\gamma \rightarrow e b\bar{b}$ rate.

A further background considered in [7], is the resolved $e\gamma(g) \rightarrow e b\bar{b}$ production, where the photon interacts via its gluonic content. Although the gluon distribution of the photon is presently poorly known, this possible background has also been investigated, and should not be competitive with the previous channels.

One of the advantages of a linear collider is the possibility to work with polarized beams.

This may allow, on the one hand, to test the parity structure of the interactions governing a particular process and, on the other hand, to optimize its background suppression. Hence, we considered the possibility of having either the electron or the photon beam longitudinally polarized. In table 2, the e/γ polarization dependence of the total cross section, its $\gamma\gamma H$, $Z\gamma H$ and BOX components, and the interference pattern of the $\gamma\gamma H$, $Z\gamma H$ and BOX contributions are shown for $p_T^e > 100\text{GeV}$, at $\sqrt{s} = 500\text{GeV}$ and different values of m_H . The total rates turns out to be very sensitive to the electron polarization, in the high p_T^e sector of the phase-space. For instance, assuming $P_e = -1$ ($P_e = +1$) the total cross section increases (decreases) by about 94% at $\sqrt{s} = 500\text{GeV}$. For $P_e = +1$ there is a strong destructive interference between the terms $\gamma\gamma H$ and $Z\gamma H$. This is essentially due to the different sign of the couplings $ee\gamma$ and $e_R e_R Z$, where e_R stands for the right-handed electron component.

In table 1, one can also see that, although both the signal S and background B are increased by a left-handed e polarization, the ratio S/B is improved at large p_T^e .

The effect of a longitudinally polarized photon beam is similar to the e polarization, but is quantitatively more modest, especially at large values of \sqrt{s} . One exception is given by the BOX contribution that is still considerably altered by $P_\gamma \neq 0$ at any \sqrt{s} [7].

Important improvements in the S/B ratio can be obtained by exploiting the final-electron angular asymmetry of the signal (figure 8), by measuring the difference between the forward and backward cross sections. A detailed analysis of this optimization procedure can be found in [7]. With a luminosity of 100 fb^{-1} , at $\sqrt{s} = 500\text{GeV}$, one expects an accuracy as good as about 10% on the measurement of the $Z\gamma H$ effects. A luminosity of 50 fb^{-1} would anyhow allow to measure the standard model signal with an accuracy better than 20%.

References

- [1] J.F. Gunion, H.E. Haber, G. L. Kane and S. Dawson, *The Higgs Hunter's Guide* (Addison-Wesley, New York, 1990).
- [2] J. Ellis, M.K. Gaillard and D.V. Nanopoulos, Nucl. Phys. B106 (1976) 292; M.A. Shifman, A.I. Vainshtein, M.B. Voloshin, V.I. Zakharov, Sov. J. Nucl. Phys. 30 (1979) 711.
- [3] L. Bergstrom and G. Hulth, Nucl. Phys. B259 (1985) 137; ERRATUM *ibid* B276 (1986) 744.
- [4] F. Wilczek, Phys. Rev. Lett. 39 (1977) 1304.
- [5] J.F. Gunion and H.E. Haber, Phys. Rev. D48 (1993) 5109; O.J.P. Eboli, M.C. Gonzales-Garcia, F. Halzen and D. Zeppenfeld, Phys. Rev. D48 (1993) 1430; D.L. Borden, D.A. Bauer and D.O. Caldwell, Phys. Rev. D48 (1993) 4018;

D.L. Borden,, V.A. Khoze, W.J. Stirling and J. Ohnemus, Phys. Rev. D50 (1994) 4499;
M. Baillargeon, G. Belanger and F. Boudjema, Phys. Rev. D51 (1995) 4712.

- [6] I. Watanabe, Proceedings, *Physics e^+e^- , $e\gamma$ and $\gamma\gamma$ collisions at linear accelerators*, Tokyo 1994, 139-148, hep-ph/9504226.
- [7] E. Gabrielli, V.A. Ilyin and B. Mele, hep-ph/9702414, submitted to Phys. Rev. D.
- [8] C.F. von Weizsäcker, Z. Phys. 88(1934) 612;
E.J. Williams, Phys. Rev. 45 (1934) 729.
- [9] O.J.P. Èboli and M.C. Gonzales-Garcia, Phys. Rev. D49 (1994) 91.
- [10] A. Barroso, J. Pulido and J.C. Romao, Nucl. Phys. B267 (1985) 509; B272 (1986) 693.
- [11] A. Abbasabadi, D. Bowser-Chao, D.A. Dicus and W.A. Repko, Phys. Rev. D52 (1995) 3919.
- [12] A. Djouadi, V. Driesen, W. Hollik and J. Rosiek, Nucl. Phys. B491 (1997) 68.
- [13] U. Cotti, J.L. Diaz-Cruz, J.J. Toscano, hep-ph/9704304.
- [14] P.A. Baikov at al., Proceedings, X Workshop on *High Energy Physics and Quantum Field Theory* (QFTHEP-96), Moscow 1996, ed. B. Levchenko and V. Sarin, hep-ph/9701412;
E.E. Boos, M.N. Dubinin, V.A. Ilyin, A.E. Pukhov and V.I. Savrin, preprint SNUTP-94-116, Oct 1994 and Korean Physical Society meeting, Oct 21, 1994, hep-ph/9503280.

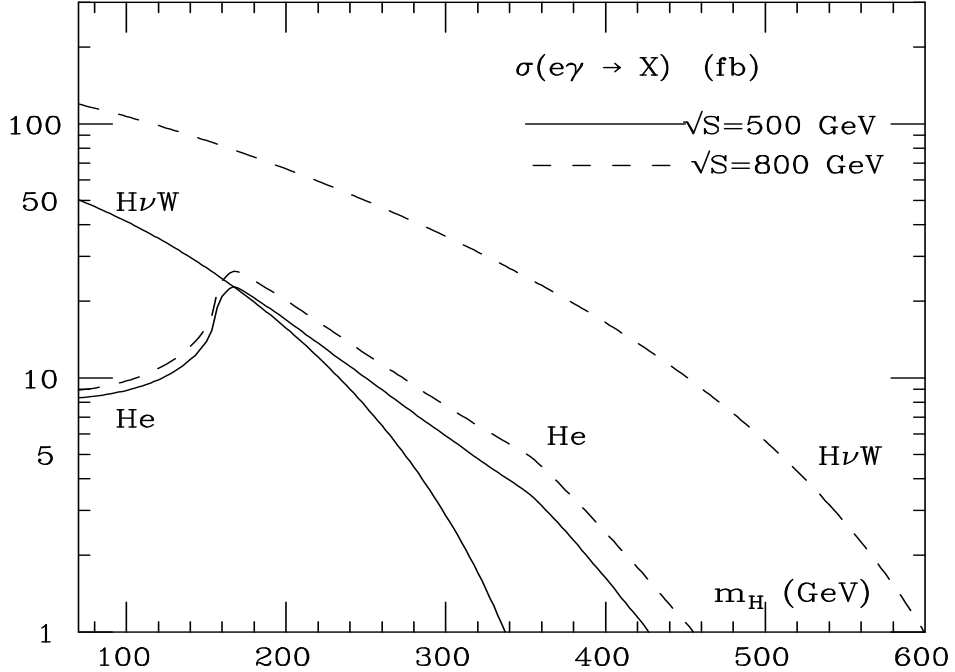


Figure 6: Total cross sections for the two main H production processes.

$m_H = 120 \text{ GeV}$ $\sqrt{s} = 500 \text{ GeV}$	$p_T^e > 100 \text{ GeV}$			$p_T^e > 10 \text{ GeV}$		
	$\sigma(eH) \text{ (fb)}$	$\sigma(ebb) \text{ (fb)}$	$\sigma(ecc) \text{ (fb)}$	$\sigma(eH) \text{ (fb)}$	$\sigma(ebb) \text{ (fb)}$	$\sigma(ecc) \text{ (fb)}$
$P_e = 0$	0.530	0.634	0.208	1.17	1.34	0.868
$P_e = -1$	1.03	0.961	0.277	1.89	1.94	1.00
$P_e = +1$	0.0249	0.304	0.136	0.422	0.767	0.726

Table 1: Comparison of the signal with the irreducible background $e\gamma \rightarrow e\bar{b}b$ and the reducible background coming from $e\gamma \rightarrow ec\bar{c}$, for different e-beam polarizations. For the $e\gamma \rightarrow ec\bar{c}$ background, a 10% probability of misidentifying a c quark into a b is assumed (that is, only 1/10 of the cross section is reported). Two configurations for kinematical cuts are considered. The angular cut $\theta(b(c) - \text{beam}) > 18^\circ$ is applied everywhere. The signal rates includes the complete treatment of the $H \rightarrow b\bar{b}$ decay. The $b\bar{b}$ invariant mass for the background is integrated over the range $m_H - \Delta m_{b\bar{b}} < m_{b\bar{b}}(m_{c\bar{c}}) < m_H + \Delta m_{b\bar{b}}$, with $\Delta m_{b\bar{b}} = 3 \text{ GeV}$.

$\sqrt{s} =$ 500GeV	m_H (GeV)	$\sigma(e\gamma \rightarrow eH, p_T^e > 100 \text{ GeV}) \text{ (fb)}$						
		Total	$ \gamma\gamma H ^2$	$ Z\gamma H ^2$	$ \text{box} ^2$	Int. $_{(\gamma\gamma H-Z\gamma H)}$	Int. $_{(\gamma\gamma H-\text{box})}$	
$(P_e = 0;$ $P_\gamma = 0)$	80	0.618	0.264	0.146	0.0451	0.0389	0.0651	0.0585
	100	0.652	0.277	0.154	0.0481	0.0409	0.0695	0.0625
	120	0.705	0.296	0.166	0.0532	0.0439	0.0766	0.0692
	140	0.818	0.341	0.190	0.0633	0.0505	0.0909	0.0822
$(P_e = -1;$ $P_\gamma = 0)$	80	1.20	0.264	0.176	0.0899	0.423	0.124	0.122
	100	1.27	0.277	0.185	0.0959	0.445	0.133	0.130
	120	1.37	0.296	0.199	0.106	0.478	0.147	0.144
	140	1.59	0.341	0.228	0.126	0.549	0.174	0.171
$(P_e = +1;$ $P_\gamma = 0)$	80	0.0371	0.264	0.117	3.55E-04	-0.345	5.86E-03	-4.94E-03
	100	0.0386	0.277	0.123	3.66E-04	-0.363	6.21E-03	-5.22E-03
	120	0.0405	0.296	0.133	3.82E-04	-0.390	6.72E-03	-5.65E-03
	140	0.0465	0.341	0.152	4.10E-04	-0.448	7.62E-03	-6.36E-03
$(P_e = 0;$ $P_\gamma = -1)$	80	0.796	0.264	0.153	0.0798	0.118	0.0903	0.0901
	100	0.852	0.277	0.162	0.0860	0.131	0.0986	0.0983
	120	0.940	0.296	0.175	0.0962	0.149	0.112	0.112
	140	1.12	0.341	0.201	0.116	0.182	0.138	0.137
$(P_e = 0;$ $P_\gamma = +1)$	80	0.440	0.264	0.139	0.0104	-0.0403	0.0399	0.0268
	100	0.452	0.277	0.146	0.0103	-0.0487	0.0403	0.0267
	120	0.470	0.296	0.157	0.0101	-0.0610	0.0411	0.0268
	140	0.520	0.341	0.179	0.0101	-0.0812	0.0434	0.0275

Table 2: *Interference pattern between the $\gamma\gamma Z$, $Z\gamma H$ and boxes contributions versus the e -beam and γ -beam polarizations, for $p_T^e > 100 \text{ GeV}$.*

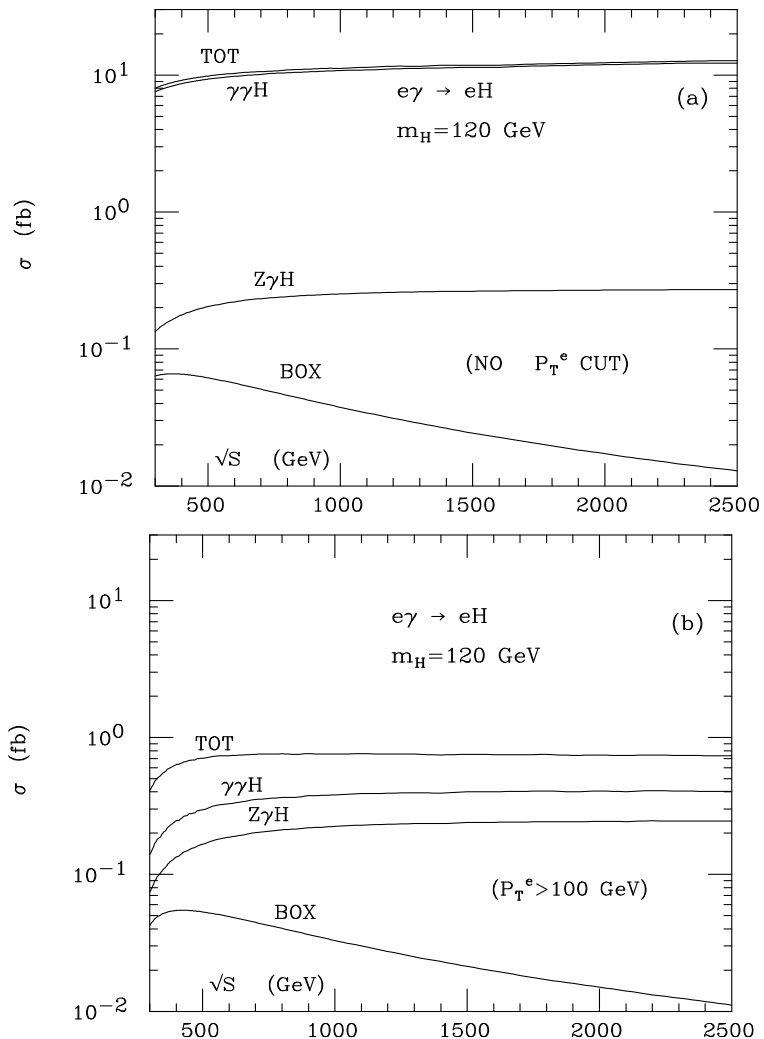


Figure 7: Effect of imposing a p_T^e cut on the $e\gamma \rightarrow eH$ cross section.

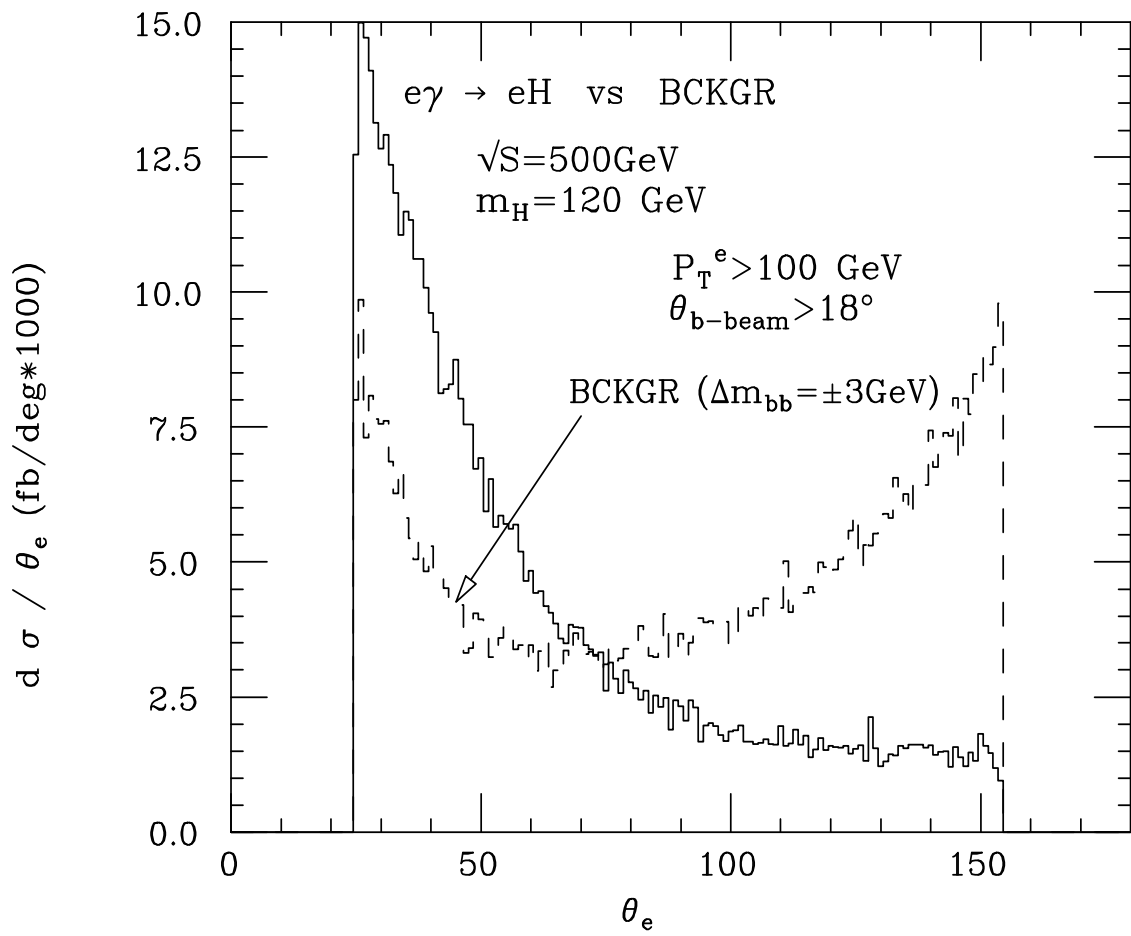


Figure 8: Final electron angular distribution with respect to the initial electron beam. The solid (dashed) line refers to the signal (irreducible $e\gamma \rightarrow ebb$ background). The kinematical cuts applied are shown in the plot. The initial beams are assumed to be unpolarized.